

SENSITIVITY OF DMLS MACHINING STEEL FATIGUE STRENGTH TO BUILD ORIENTATION AND ALLOWANCE FOR MACHINING

Dario Croccolo ¹, Massimiliano De Agostinis ¹, Stefano Fini ¹, Giorgio Olmi ¹, Francesco Robusto ¹, Snežana Ćirić Kostić ², Slobodan Morača ³, Nebojša Bogojević ²

¹ Department of Industrial Engineering (DIN), University of Bologna, Bologna, Italy

² Faculty of Mechanical and Civil Engineering in Kraljevo, University of Kragujevac, Serbia

³ Department of Mechanical Engineering, Faculty of Technical Sciences, University of Novi Sad, Serbia

Corresponding Author:

Eng. Giorgio Olmi, Ph.D.

Department of Industrial Engineering (DIN)

University of Bologna

Viale del Risorgimento, 2 - 40136 BOLOGNA (BO) - ITALY

Phone: +39 051 2093455, +39 0543 374427 (in Forlì)

Fax: +39 051 2093412

E - mail: giorgio.olmi@unibo.it

ABSTRACT

This work deals with the effect of build orientation and of allowance for machining on DMLS produced Maraging Steel MS1. The experimental results, arranged by tools of Design of Experiment, have been statistically processed and compared. The outcomes were that, probably due to effect of the thermal treatment, machining and material properties, the aforementioned factors do not have a significant impact on the fatigue response. This made it possible to work out a global curve that accounts for all the results, consisting in a high amount of data points. This can be regarded as one of the most complete and reliable fatigue models in the current literature. Fractographic and micrographic studies have been performed as well, to individuate the crack initiation points, usually located at sub-surface porosities, and to investigate the location of internal inclusions and the actual martensitic microstructure along the stacking direction and on the build plane.

Keywords: Additive Manufacturing, DMLS, Maraging Steel, Rotating Bending Fatigue, Build orientation, Allowance for Machining.

NOMENCLATURE

AM Additive Manufacturing

ANOVA Analysis of Variance

CAD Computer Aided Design

CTE Coefficient of thermal expansion

DMLS Direct Metal Laser Sintering

FL Fatigue Limit [MPa]

R Stress Ratio (fatigue tests)

f Frequency (fatigue tests) [Hz]

R_a Roughness Average [μm]

S_i 10-base logarithm of σ_i

\bar{S} Overall mean (for ANOVA)

SLM Selective Laser Melting

S-N curve Maximum Bending Stress vs. Life Cycles curve in the finite life domain

SSBC Sum of Squares between Columns (for ANOVA)

SSE Sum of Squares Error (for ANOVA)

SSI Sum of Squares Interaction (for ANOVA)

SSBR Sum of Squares between Rows (for ANOVA)

UTS Ultimate Tensile Strength [MPa]

σ_i Finite life fatigue strength for the (i- th) sample set

INTRODUCTION

Nowadays, Additive Manufacturing (AM) technologies are attracting a remarkable interest from industry, civil constructions and academia, considering its great potentials and its large applications. AM makes it possible to achieve the production of even much complicated geometries directly from three-dimensional CAD (computer aided design) models in a short time¹, thus remarkably reducing the time from conception to market. A high flexibility arises from this point, considering also this process allows for a reduced waste of powder material, in addition there is often no need for expensive molds or tools for part production. These features make it possible to compensate the high costs for machines and for raw powder material supply. Moreover, through a full exploitation of metal AM technique, lighter parts can be obtained: the capability of building even highly complicated shapes, which would not be affordable by conventional production methods, makes it possible to significantly increase the strength to weight ratio. This technique is more and more used in many strategic fields, e.g. automotive, aerospace, as well in the biomedical and injection molds industries¹⁻².

The most widely used techniques of AM for metals are Selective Laser Melting (SLM) that emphasizes the use of a laser as energy source, and Direct Metal Laser Sintering (DMLS) that also makes use of a laser to selectively sinter some solid areas of the cross section of the built part. Nowadays, these two techniques can be regarded as being basically the same, according to³⁻⁶. Both have the capability of building metal parts layer-by-layer, starting from a highly controlled metal powder⁷⁻⁸. The CAD 3D model is initially split into several slices, individuating the cross sections corresponding to each slice. This makes it possible to convert a 3D problem into a 2D one. Afterwards, a high-power laser is used to selectively fuse metallic powder particles, by some scans with controlled direction, which generate the solid shape of the part. After the consolidation of one powder layer, a new powder layer is stacked, the base plate is moved downwards, and the aforementioned process is repeated until the completion of the component. During this building process, a large part of metal powder is generally unused, but can then be recycled, which makes it possible to strongly reduce the waste of raw material.

However, AM techniques also have some drawbacks arising from their typical cast structure, involving high surface roughness, presence of pores or sometimes oxides and thermal tensile residual stresses. These are due to remarkably steep temperature gradients affecting the layers and significant cooling rates. Despite these outcomes, previous studies in the literature, as well as data sheets by powder producers, indicate that their monotonic properties can be well comparable to those of wrought material, with an isotropic response regardless of the build orientation during the stacking process. Anyway, a further issue with AM processed parts arises from the lack of a sufficiently high amount of studies dealing with their fatigue properties, considering that this is the most frequent state of load in the previously mentioned application fields.

Several papers dealing with this topic are focused on Ti-6Al-4V, one of the first materials to be made available for powder bed fusion technologies and with many applications in the aerospace and in prosthesis fabrication. For instance, the studies⁹⁻¹⁰ investigated the fatigue response of SLM produced notched samples, to be compared to that of smooth parts and of plain wrought material¹¹. The fatigue data were analyzed in the light of extensive environmental scanning electron microscope observation, in order to compare the different failure mechanisms, depending on sample fabrication strategy.

According to the literature ¹² the fatigue limit is often coarsely estimated as the 50% of the ultimate tensile strength (UTS) of the material, considering conventional subtractive manufacturing. The determination of a correct fatigue limit to UTS ratio for additively produced parts is still under investigation.

Maraging steels are particularly suitable to powder bed fusion manufacturing techniques, such as DMLS or SLM ¹³. Moreover, they exhibit a high performance in terms of UTS (close to 2,000 MPa, following aging treatment, regardless of the build orientation ¹⁴) and of fracture toughness, which makes them promising materials in many fields. However, a possible issue is that a lack of studies, specifically dealing with the fatigue response of this material, can be still observed in the scientific literature. A previous research ¹⁵ investigated the fatigue response (in terms of both the fatigue strength in the finite life domain and the fatigue limit) of Maraging steel MS1 (also reported as 18% Ni Maraging 300 or AISI 18Ni300). An experimental campaign was aimed at the investigation of the potential impact of the build orientation on fatigue, following heat aging treatment and machining with 0.5 mm allowance. In particular, three sets of samples were considered, with horizontal, vertical and slanted (45° inclined) build orientation with respect to the base plate in the chamber. The heat treatment and machining post-manufacture procedures were kept unchanged for the three sample batches. The outcome was that the results, processed by International Standards, were all well comparable for the three build orientations and the estimated fatigue limit was around 590 MPa, corresponding to 29% of the UTS. Consequently, the post manufacture treatments (aging and machining) proved to be able to remove any source of anisotropy. The determined fatigue limit to UTS ratio was also consistent with those of the experimental campaigns described in ¹⁶⁻²⁰ that dealt with Maraging steels in wrought conditions. A recent study ²¹ has been focused on the effect of the laser scan speed on both static and fatigue performance, as well as on the porosities induced in the microstructure. However, the tests were conducted under subsequent blocks with different stress range and are therefore not comparable to the previous ones. Moreover, one build orientation only (vertical with respect to the powder bed) has been considered. Other studies, e.g. ², are mainly focused on the static properties or on the effect of the process parameters on the achieved microstructure of AM processed Maraging steel parts ²². An interesting and particularly recent study is presented in ¹, where AISI 18Ni300 samples were involved in a quite extensive low-cycle fatigue campaign. However, this study was more oriented to the elasto-plastic behaviour in the low-cycle fatigue domain, rather than to the fatigue response in the nominally elastic field and to its dependence on build or post-process parameters.

The subject of the present study consists in an extension of the outcomes of ¹⁵: it aims at investigating the build orientation effect for increased allowance for machining, and then to better investigate the potential effect of allowance on the fatigue strength of the built and then machined components. The parts have all been produced by DMLS using a commercial machine by EOS. These two goals have been tackled by designing a suitable experimental campaign that completes and integrates the previous one described in ¹⁵. Regarding the study on allowance, motivations stem from some recent researches ²³⁻²⁵, which are starting to focus on the so called “size effect”, i.e. the effect of the amount of material to be removed after sintering on mechanical properties. The here reported results indicate a remarkably slower crack growth rate, following machining from oversized blocks. The fatigue performance of machined Ti-6Al-4V samples with suitable selection of allowance has also been the topic of the study ²⁶, which confirms the general interest in this point. A recent study ³ has been focused on the effect of allowance on fatigued 15-5 PH Stainless steel,

reporting a beneficial effect of the incremented allowance. This is presumably due to the removal of the superficial layers around the contour, where the concentration of voids is statistically higher, and to the drop of residual stresses.

EXPERIMENTAL METHOD

The experimental campaign involved Maraging steel MS1 (also reported as 18% Ni Maraging 300 or AISI 18Ni300), whose chemical composition is provided in Table 1. The material powder was supplied by EOS GmbH – Electro Optical Systems, Krailling/Munich, Germany). Fatigue testing was carried out under rotating bending, following the Standard ISO 1143. Specimen geometry was chosen accordingly, with reference to the cylindrical smooth shape with uniform cross section at gage. The samples were manufactured with 6 mm diameter at gage and 10 mm diameter at the heads as a good compromise to reduce production costs, while ensuring agreement with the Standard. The gage length was 20.6 mm and the length of the reduced section, including 25 mm radius fillets, was 40 mm.

Table 1: Chemical composition (weight percentage) of Maraging steel MS1

Ni [%]	Co [%]	Mo [%]	Ti [%]	Al [%]	Cr [%]	Cu [%]	C [%]	Mn [%]	Si [%]	P [%]	S [%]	Fe [%]
17-19	8.5-9.5	4.5-5.2	0.6-0.8	0.05-0.15	≤ 0.5	≤ 0.5	≤ 0.03	≤ 0.1	≤ 0.1	≤ 0.01	≤ 0.01	Bal.

The specimens were manufactured by EOSINT M280 system (EOS GmbH - Electro Optical Systems, Krailling/Munich, Germany), equipped with Ytterbium fiber laser with 200W power and emitting 0.2032mm thickness and 1064nm wavelength infrared light beam. The process took place in an inert environment in a working space with 250 × 250 mm dimensions on the horizontal plane and a maximum height of 325 mm. The layer thickness was set to 40 μm and a parallel scan strategy with alternating scan direction was adopted. This direction was rotated by 70° at every layer, to get a better structure uniformity. Moreover, a contour line was scanned at every layer to better define the external shape.

Table 2: Design of the experimental campaign

		Allowance [mm]				
		0.5	1.0	2.0	3.0	4.0
Build orientation	Horizontal	Set #2 (H,0.5)			Set #4 (H,3)	
	Vertical	Set #1 (V,0.5)	Set #7 (V,1)	Set #8 (V,2)	Set #6 (V,3)	Set #9 (V,4)
	Slanted	Set #3 (S,0.5)			Set #5 (S,3)	

The experimental campaign was arranged according to Table 2 that takes two parameters into account: build orientation and allowance. In particular, three levels were considered for the first factor: horizontal, vertical, and slanted (45° inclined) with reference to the inclination of the sample main axis of inertia with respect to the horizontal base plate during the deposition process with vertical stacking direction. Regarding the allowance factor, it refers to the allowance accounted during the machining task at every sample gage. Five levels were considered: 0.5, 1, 2, 3 and 4 mm. For the sake of clarity, consistently with the study³, a double notation has been used: the sample Sets have been identified by both their sequential number and a letter (H for horizontal, V for vertical, and S for slanted), followed by a number indicating the entity of allowance. It is worth mentioning that this study must be regarded as a follow-up of the previous one included in ¹⁵: in particular, the sets with numbers 1-3 were included in that previous research. The current one has dealt with sets #4 to #9, to investigate the effect of the build orientation at incremented (3 mm)

allowance and to then deepen the study on allowance for fixed (vertical) build orientation. The blank boxes indicate not investigated treatment combinations, due to their reduced interest for production and design purposes.

After the building process and before machining all the samples underwent the recommended surface and heat treatments by the powder producer. In particular, they were treated by micro-shot-peening, in order to close the pores that may be induced by laser sintering. Stainless steel spherical shots, with 400 μ m diameter, under 5 bar flow pressure, were utilized for this purpose. Afterwards, an aging heat treatment, consisting in age-hardening at 490°C for 6 hours ¹⁴ was conducted. This treatment is typically aimed at reducing the tensile residual stresses, arising from the stacking process. The DMLS component in the “as fabricated” state consists of a majority of martensite (α) phases and a small minority of austenite (γ) phases. According to ²⁷, the volumetric percentages are respectively 89.7% and 10.3%. Following the aforementioned aging treatment, the relative amount of γ phase is slightly increased up 11%, while the percentage of α phase is correspondingly dropped to 89%. Finally, the specimens underwent machining and refining by grinding with the aim of accomplishing the roughness and dimensional specifications and of improving the fatigue performance.

The fatigue testing was aimed at the determination of the S-N curves and the fatigue limits (FLs). An abbreviated staircase method was applied to determine the FL, according to the Dixon method ²⁸⁻³¹. A life duration of 10⁷ cycles was set as run-out, as suggested by the literature and in accordance with ¹⁵. A confidence analysis (90% confidence level) was also performed based on the standard deviation of FL (scattering of the experimental results) and on the size of the sequence that led to its computation. The data in the finite life domain were processed according to the Standard ISO 12107 ³²: both the linear and the quadratic model have been worked out and the general linear test has then been applied, to assess the significance of the improvements arising from the latter. Lower and upper bounds to be wrapped around the curves have been determined, considering failure probabilities of 10% and 90% and with a 90% confidence level. The fatigue tests were carried out in the stress controlled mode with load ratio R=-1 and frequency f=60Hz, so that each sample was loaded under a four-point rotary bending configuration with constant maximum nominal bending moment at gage.

The experimentation was preceded by dimensional checks and roughness measurements that involved every sample. For this purpose, a micrometre screw gage, a digital calliper (both with the resolution of 0.01mm) and a portable surface roughness tester (with the resolution of 0.01 μ m, Handysurf E-30A; Carl Zeiss AG, Oberkochen, Germany) were used. Measurements were carried out with 4 replications at each head and with 6 replications at gage. The sample diameter was measured along 90° angled direction. As for roughness, Ra was retrieved considering again 90° angled spots, averaging the roughness profiles over a 4 mm tester shift. Measurements related to the Set #6 (V, 3) are collected in Table 3. Some roughness measurements at the gage are missing, when the related sample survived the fatigue testing: in this cases Ra at heads only was retrieved, due to the impossibility to correctly align the roughness tester at the gage for unbroken samples. At the end of the fatigue testing, crack surfaces were carefully analysed for the individuation of the crack nucleation point and of internal defects, such as oxides or porosities. For this purpose, a Stemi 305 stereo-microscope (by ZEISS, Oberkochen, Germany) as well as an Optiphot-100 optical microscope (by Nikon, Melville, NY, United States) have been utilized. Micrographies have also been performed, performing cuts of the samples along the cross section and along their longitudinal direction, thus

individuating the microstructure along the build direction and on the deposition plane. After proper surface texturing, chemical etching (for 1 min 20 s at room temperature) has been performed, according to the following recipe: 150ml H₂O, 50ml HCl, 25ml HNO₃, 1g CuCl₂. The samples have then been observed by the aforementioned optical microscope.

Table 3: Dimensional and roughness (R_a) measurements with regard to the samples of Set #6

Specimen ID	Gage diameter			Head diameter (left side)			Head diameter (right side)		
	Mean [mm]	St. dev. [mm]	Roughness Ra [μm]	Mean [mm]	St. dev. [mm]	Roughness Ra [μm]	Mean [mm]	St. dev. [mm]	Roughness Ra [μm]
6.1	6.00	0.008	0.819	10.02	0.001	0.315	10.01	0.001	0.275
6.2	6.00	0.008	0.785	10.01	0.002	0.295	10.02	0.001	0.269
6.3	6.00	0.008	0.758	10.01	0.002	0.294	10.02	0.000	0.293
6.4	5.99	0.010	---	10.02	0.001	0.304	10.02	0.001	0.271
6.5	6.00	0.007	0.779	10.01	0.002	0.336	10.02	0.002	0.305
6.6	6.00	0.013	0.738	10.01	0.002	0.388	10.02	0.002	0.286
6.7	5.99	0.009	---	10.01	0.002	0.294	10.02	0.000	0.309
6.8	5.99	0.006	0.748	10.02	0.002	0.331	10.02	0.001	0.330
6.9	5.99	0.007	0.736	10.01	0.002	0.320	10.02	0.001	0.286
6.10	6.00	0.007	0.733	10.01	0.002	0.346	10.01	0.002	0.286
6.11	6.00	0.007	0.733	10.01	0.003	0.313	10.02	0.001	0.261
6.12	5.99	0.007	0.745	10.02	0.001	0.353	10.01	0.000	0.270
6.13	6.00	0.008	0.769	10.02	0.002	0.404	10.01	0.001	0.308

RESULTS

The results of the fatigue tests for sample Sets #1 to #9 are collected in Table 4: in particular, sample identifier, the applied load (in terms of maximum nominal bending stress at the gage, corresponding to the nominal bending stress amplitude of the fatigue cycle) and the observed life (in terms of cycles to failure) are provided.

Table 4: Results of the fatigue testing campaign (including results in ¹⁵)

Specimen ID	Stress amplitude [MPa]	Cycles to Failure	Failure / Run-out	Specimen ID	Stress amplitude [MPa]	Cycles to Failure	Failure / Run-out
1.1	699	2,277,295	Failure	3.5	699	3,582,162	Failure
1.2	665	3,374,203	Failure	3.6	665	4,309,539	Failure
1.3	596	6,090,458	Failure	3.7	550	---	Run-out
1.4	524	---	Run-out	3.8	579	---	Run-out
1.5	560	---	Run-out	4.1	759	554,382	Failure
1.6	560	---	Run-out	4.2	700	3,435,461	Failure
1.7	596	---	Run-out	4.3	670	387,562	Failure
2.1	699	3,780,607	Failure	4.4	640	5,642,058	Failure
2.2	665	4,926,903	Failure	4.6	580	---	Run-out
2.3	579	---	Run-out	4.7	610	8,255,277	Failure
2.4	610	8,225,283	Failure	4.8	580	9,289,822	Failure
2.6	579	---	Run-out	4.9	550	9,472,904	Failure
2.7	610	9,262,114	Failure	4.10	550	---	Run-out
3.3	550	---	Run-out	5.1	700	3,499,346	Failure
3.4	579	8997765	Failure	5.2	670	6,092,545	Failure

Specimen ID	Stress amplitude [MPa]	Cycles to Failure	Failure / Run-out	Specimen ID	Stress amplitude [MPa]	Cycles to Failure	Failure / Run-out
5.3	639	4,554,231	Failure	7.5	579	4,263,093	Failure
5.4	610	---	Run-out	7.6	550	8,686,316	Failure
5.5	639	8,214,794	Failure	7.7	520	---	Run-out
5.6	610	9,367,065	Failure	7.8	550	8,308,210	Failure
5.7	580	9,612,600	Failure	7.9	520	---	Run-out
5.8	550	---	Run-out	8.1	759	2,173,992	Failure
5.9	760	1,807,539	Failure	8.2	699	3,681,461	Failure
5.10	820	503,537	Failure	8.3	639	7,003,462	Failure
6.1	759	3,411,585	Failure	8.4	580	9,426,902	Failure
6.2	700	5,499,068	Failure	8.5	550	---	Run-out
6.3	640	7,468,459	Failure	8.6	580	9,074,564	Failure
6.4	610	---	Run-out	8.7	550	---	Run-out
6.5	640	8,456,821	Failure	8.8	580	9,901,534	Failure
6.6	610	7,982,955	Failure	8.9	610	5,153,485	Failure
6.7	579	---	Run-out	8.10	821	1,609,415	Failure
6.8	610	8,247,250	Failure	9.1	759	2,643,707	Failure
6.9	881	445,085	Failure	9.2	699	3,483,595	Failure
6.10	881	243,461	Failure	9.3	639	5,671,878	Failure
6.11	821	1,265,354	Failure	9.4	579	---	Run-out
6.12	821	1,591,045	Failure	9.5	610	5,586,420	Failure
6.13	579	6,547,376	Failure	9.6	579	---	Run-out
7.1	759	1,664,344	Failure	9.8	610	7,388,578	Failure
7.2	699	2,716,753	Failure	9.9	579	---	Run-out
7.3	639	4,854,824	Failure	9.10	821	1,171,227	Failure
7.4	610	2,733,629	Failure				

As mentioned above, the fatigue curve in the finite lifespan domain were processed according to the Standard ISO 12107³² through the determination of both the linear and the quadratic models. As recommended, the tools of the Residuals Plot and of the Normal Probability Plot have been utilized, to individuate and exclude the possible outliers. The general linear test always led to the outcome that the improvements yielded by the latter were not significant. Therefore, the linear model proved to be the most suitable to process all the results. The fatigue curves can be expressed as in Eq. (1) or Eq. (2),

$$\text{Log}(N) = b_0 + b_1 \cdot \text{Log}(\sigma_i) \quad (1)$$

$$\sigma_i = 10^{\frac{b_0}{b_1}} \cdot N^{\frac{1}{b_1}} \quad (2)$$

whose coefficients are expressed in Table 5 for each sample set

Table 5: Coefficients of the determined S-N curves, according to the linear model of ³², with reference to Eqs. (1-2)

Set #	b_0	b_1	$10^{-\frac{b_0}{b_1}}$	$\frac{1}{b_1}$
1	23.56	-6.04	7,928	-0.165
2	24.31	-6.24	7,904	-0.160
3	20.71	-4.98	14,383	-0.201
4	29.87	-8.28	4,038	-0.121
5	30.17	-8.33	4,172	-0.120
6	27.46	-7.36	5,383	-0.136
7	18.97	-4.42	19,417	-0.226
8	20.93	-5.06	13,806	-0.198
9	21.66	-5.32	11,735	-0.188

The fatigue curves for Sets #1 to 6, considering also the results in ¹⁵ are depicted in Fig. 1. The comparison of these curves makes it possible to account for the potential joint effect of build orientation and of allowance.

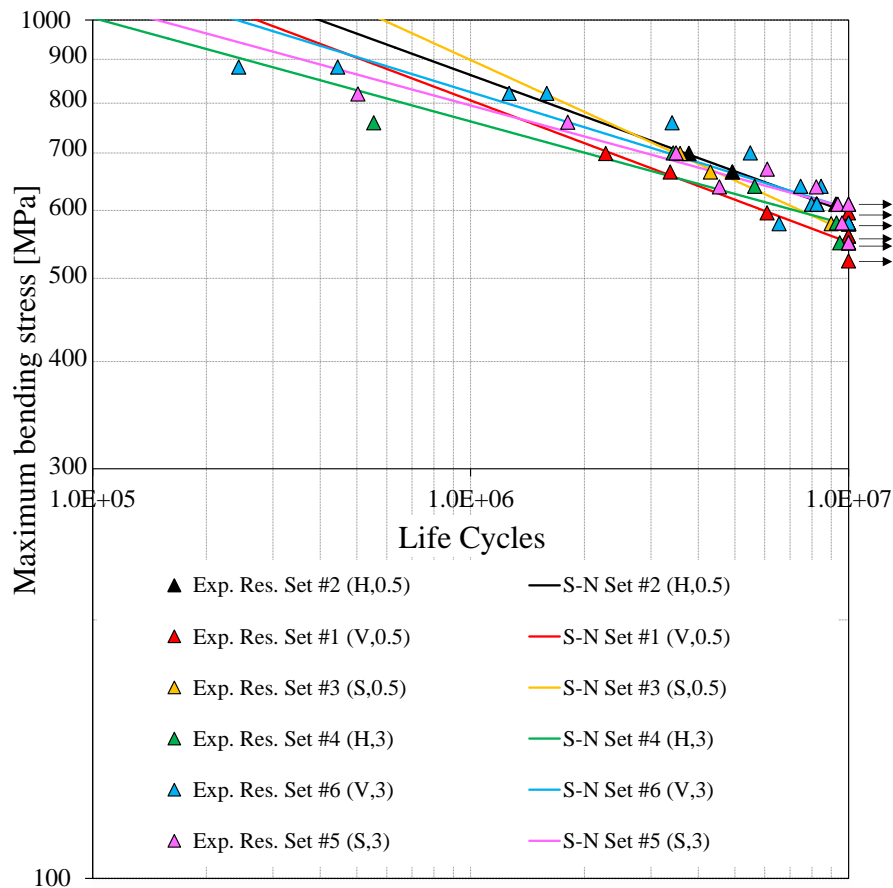


Fig. 1: S-N curves in the finite life domain for Sets #1¹⁵ to #6

The fatigue curves for Sets #1, 6, 7, 8, 9 are conversely plotted in Fig. 2. The analysis of this graph makes it possible to compare the fatigue responses at different allowance levels.

DISCUSSION

The results have been statistically processed, to assess if the differences among the curves were significant with respect to the observed scattering affecting the experimental data. For this purpose, the ANOVA-based methodology introduced and described in ^{3,33} was applied. The S-N curves related to the sets #1 to 6 were compared, regarding the related plan as a two-factor design. Conversely,

the fatigue curves with regard to Sets #1, 6, 7, 8, 9 have been compared, considering a one-factor design, to evaluate the impact of allowance for machining.

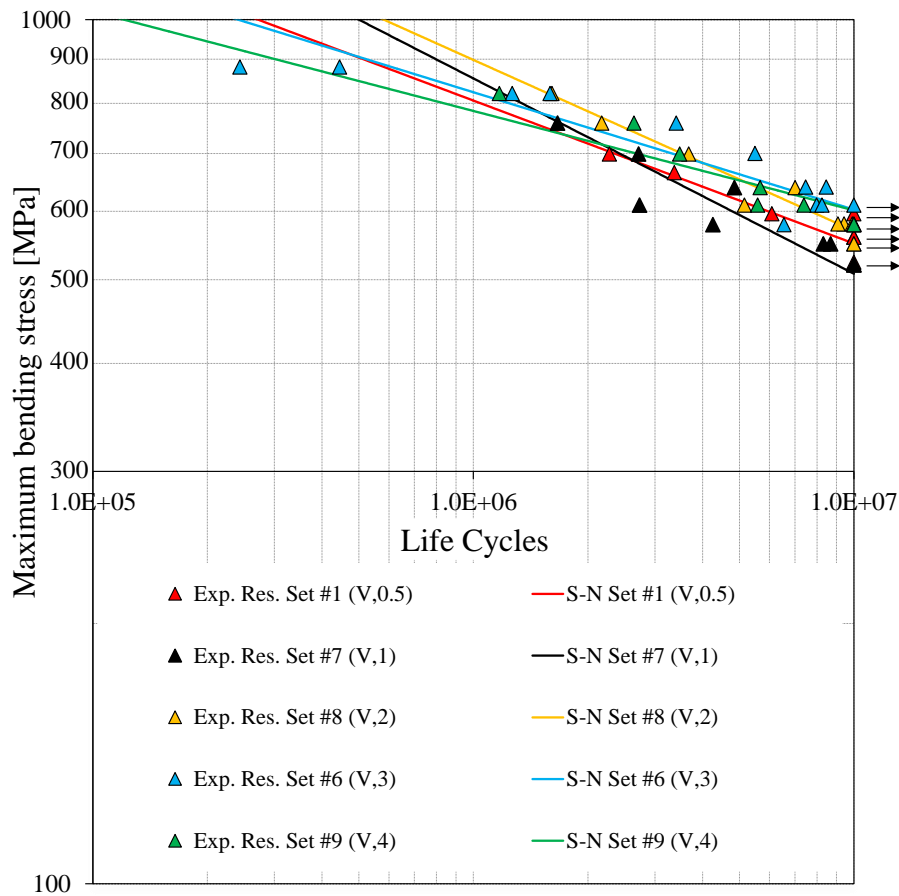


Fig. 2: S-N curves in the finite life domain for Sets #1¹⁵, 6, 7, 8 and 9

The first analysis was conducted as in ³, through the calculation of mean fatigue curves and of a grand mean fatigue curve. Then an “SSBR” term, i.e. a “Sum of squares between rows”, related to the differences among the fatigue responses for different build orientations, was computed. At the same way an “SSBC” term, i.e. a “Sum of squares between Columns” related to the effect of allowance has then estimated, to assess the difference between the fatigue responses for 0.5 and 3 mm allowance. Then, an “SSI” term, related to the interaction between the two factors was determined. All the values were converted into scalars, by calculating their integral means over the reference life span. The error-related term (“SSE”) was finally determined as the sum of the squares of the residuals between the actual experimental data and the predicted ones, based on the interpolating S-N curves.

Table 6: ANOVA Table for the two-factor design (lifespan between 10⁵ and 10⁷)

	Sum of squares	Degrees of freedom	Failure	Fisher's ratio	p-value
SSBR: Effect of the build orientation	0.0005	2	0.0003	0.44	0.65
SSBC: Effect of the thickness of allowance for machining	0.0028	1	0.0028	4.84	0.04
SSI: Interaction	0.0016	2	0.0008	1.35	0.28
SSE: Error	0.0135	23	0.0006		

All the determined yields were subsequently processed in a conventional two-factor ANOVA, provided that the aforementioned squared terms were scaled and made thus comparable one another by division by the related degrees of freedom. The analysis was conducted, considering

both an interval between 10^5 and 10^7 cycles and a more reduced lifespan between 10^6 and 10^7 . The results in both cases were that all the differences are negligible, meaning that the two factors are not significant, and that no interaction occurs. The ANOVA table regarding the first one is reported in Table 6.

The one-factor ANOVA was developed as in³³, however, considering that in this reference the analysis had been applied to a Low Cycle Fatigue study, some details are provided below for the sake of clarity. A grand mean curve $\bar{S}_{..}$ has initially been computed as in Eq. (3), where S indicates the 10-base logarithm of the stress corresponding to a generic fatigue life and the subscript refers to the Set number.

$$\bar{S}_{..} = \frac{S_1 + S_6 + S_7 + S_8 + S_9}{5} \quad (3)$$

Then, an “SSBC” term, being related to the effect of allowance, has been determined as in Eq. (4). This takes the differences among the fatigue curves for different allowance levels into account.

$$SSBC = \left[(S_1 - \bar{S}_{..})^2 + (S_6 - \bar{S}_{..})^2 + (S_7 - \bar{S}_{..})^2 + (S_8 - \bar{S}_{..})^2 + (S_9 - \bar{S}_{..})^2 \right] \quad (4)$$

As above, the error term (“SSE”) was estimated as the sum of the squares of the residuals between the experimental yields and the predicted ones, according to the interpolating fatigue curves. Scalar terms were then worked out by the integral means of the aforementioned terms. The analysis proceeded as a conventional one-factor ANOVA, provided the scalar terms were made comparable, rationalizing them by their degrees of freedom. The study was repeated for the same intervals that have been mentioned above with regard to the analysis with two factors. The outcome for the interval between 10^5 and 10^7 is provided in Table 7, in both cases the statistical test proved that the allowance does not have any effect.

Table 7: ANOVA Table for the one-factor design (lifespan between 10^5 and 10^7)

	Sum of squares	Degrees of freedom	Failure	Fisher's ratio	p-value
SSBC: Effect of the thickness of allowance for machining	0.0048	4	0.0012	1.66	0.19
SSE: Error	0.0189	26	0.0007		

This outcome is also confirmed by the computation of the fatigue limits for infinite life, considering the aforementioned run-out of 10^7 cycles. The nominal values along with their confidence intervals at the 90% confidence level, corresponding to 1.65 times the standard deviation, are displayed in the bar graph in Fig. 3. They are all quite close, with overlapped bands, except for that for Set # 7 that is a bit lower. The average value of the fatigue limit, involving the nine sets, is 581 MPa, corresponding to 28% the UTS of the studied material, following the aging treatment.

This result indicates that Maraging Steel has an isotropic behavior, moreover its response does not exhibit any significant variation for incremented allowance. In other words, this material has a particularly robust response that yields all consistent results even in different production conditions. This outcome also confirms the remarks in³. The build process of a Maraging Steel is performed with a doubled layer thickness (40 μ m instead of 20 μ m) with respect to the manufacturing of a Stainless steel. Moreover, the stacking procedure leads to a much more reduced tensile residual stress field, due to the lower coefficient of thermal expansion (CTE). In particular, the CTE of Maraging steel is approximately 10% lower than that for Stainless steel and the lower CTE, the lower the induced residual stresses^{3, 34}. The doubled value of layer thickness also affects the induced residual stress. In fact, with approximately one-half stacked layers, the state of heating/cooling is

made more uniform along the part height, and the thermal gradient as well as the residual stress state are reduced.

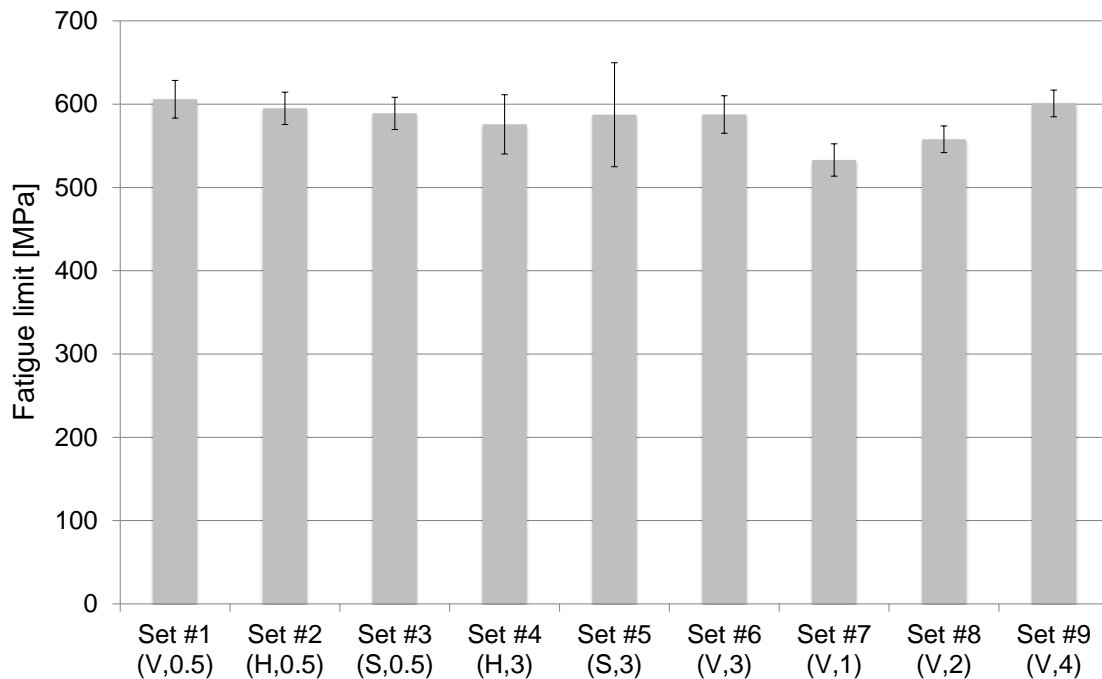


Fig. 3: Fatigue limits for 10 million cycle run-out with regard to samples #4 to 9. The results for Sets #1 to 3¹⁵ are also appended for comparison purposes.

Incremented allowance proved to have a beneficial effect for Stainless Steel, as machining was able to remove the external surface layers, thus promoting a remarkable drop of the detrimental residual stresses. For Maraging steels, residual stresses already keep a much more reduced value, therefore this beneficial effect turns to be negligible.

Moreover, due to the higher number of layers, Stainless Steel proved to be sensitive to the notch effect in case of missing scans and to the number of defects per layer due to the limited perpendicularity between the laser path and the surface. Slanted orientation proved to be the best for that material as a good compromise between a not high notch effect and a not too extended build area, which made it possible to get a good perpendicularity with the laser path, thus reducing the number of defects per layer. Maraging Steel, with one-half layers, is less sensitive to the described effects; therefore, the build orientation is also completely ineffective. Moreover, like in¹⁵, the present results confirm that the post-manufacture heat treatment and machining are able to remove any possible cause of anisotropy.

Considering the aforementioned outcomes and the statistical evidence of not significant differences among the fatigue responses of the nine sets (also including those tested in¹⁵), a global fatigue curve was determined. This curve has been yielded by the regression of all the data for all the studied sets and can be regarded as the most general and reliable description of the response of the studied Maraging Steel in the current state of the art. This model is likely to have many applications in the field of machine design, as it simultaneously accounts for the manufacturing factors of build orientation and machining and related allowance. The fatigue curve was worked out, based on the Standard ISO 12107³², by the linear model, like for all the sample sets. The confidence band at the 90% confidence level, with lower and upper bounds respectively corresponding to 10% and 90% failure probabilities, has been determined as well. The curve and the related band, along with dots corresponding to the 56 experimental data that were involved in the interpolation, is plotted in Fig. 4.

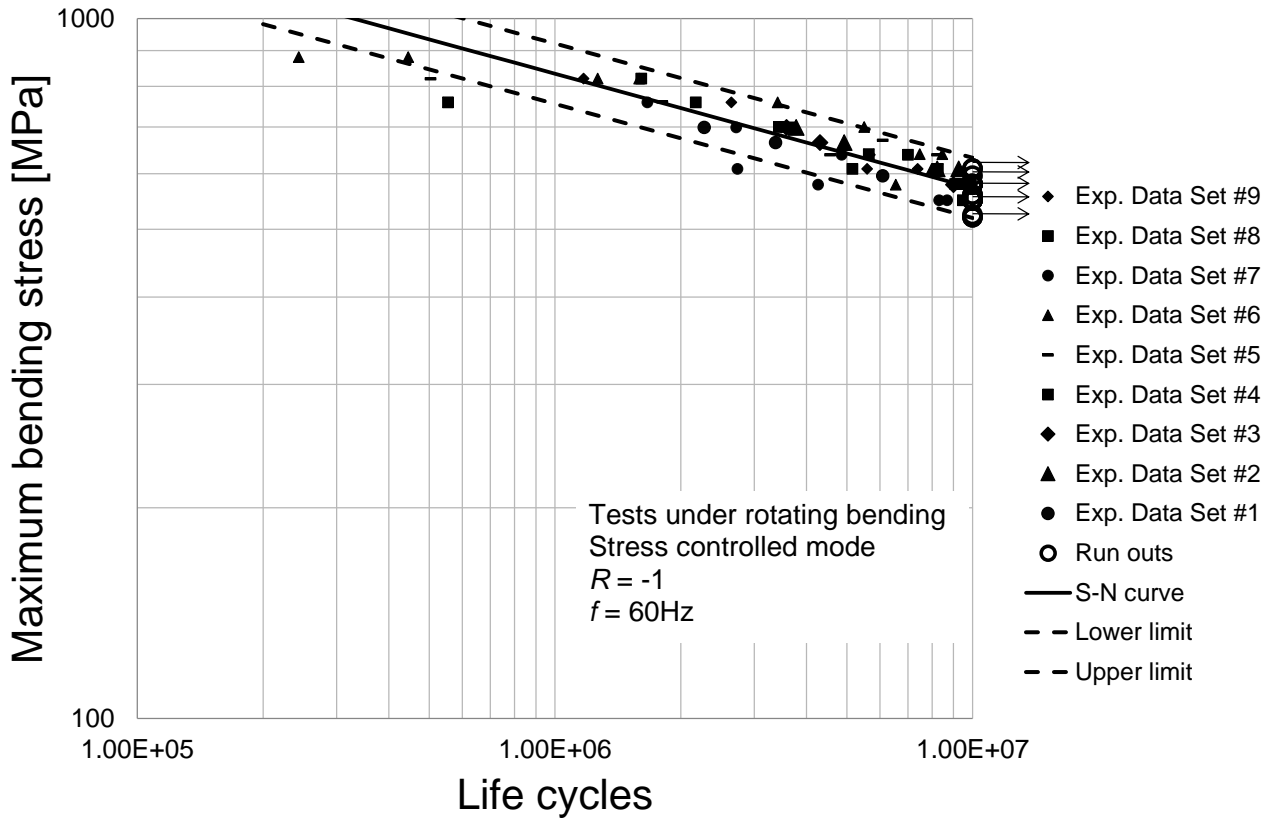


Fig. 4: Global S-N curve in the finite life domain accounting for all the 56 data

The analytical equations of the nominal curve at the 50% failure probability, to be used for life prediction, are provided in Eqs. (5-6). The equations of the aforementioned lower (10% failure probability) and upper (90% failure probability) bounds are respectively reported in Eqs. (7-8) and Eqs. (9-10).

$$\text{Log}(N) = 23.91 - 6.13 \cdot \text{Log}(\sigma) \quad (5)$$

$$\sigma = 7940 \cdot N^{-0.163} \quad (6)$$

$$\text{Log}(N) = 23.64 - 6.13 \cdot \text{Log}(\sigma) \quad (7)$$

$$\sigma = 7191 \cdot N^{-0.163} \quad (8)$$

$$\text{Log}(N) = 24.17 - 6.13 \cdot \text{Log}(\sigma) \quad (9)$$

$$\sigma = 8767 \cdot N^{-0.163} \quad (10)$$

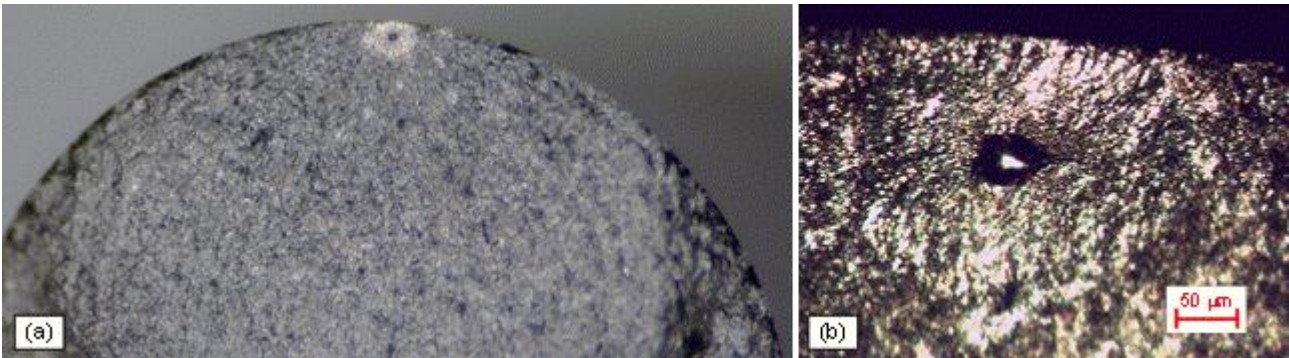


Fig. 5: Fractographic analysis of the fracture surface of sample 8.4: (a) crack initiating from a sub-surface porosity due to lack of penetration (picture by stereoscopic microscope), (b) detail of the defect (by optical microscope)

The study was finally completed by fractography. Some fracture surfaces along with details of the crack initiation points are shown in Fig. 5. It can be remarked that almost the totality of failures was

triggered by sub-surface porosities or voids with average dimension (diameter) and distance from the edge of respectively $50\mu\text{m}$ and $80\mu\text{m}$. The area of initial propagation is also made clearly visible by its bright aspect.

It is therefore clear that the failure mechanism is steered by the presence of process induced defects due to unmolten spots or lack of penetration. The described failure mode has then been compared to other ones described in the literature for AM processed parts. In particular, the studies⁹⁻¹⁰ deal with SLM fabricated Ti-6Al-4V at the unmachined state. In this case, cracks nucleated at the specimen surface, both in smooth and in notched parts, and were presumably triggered by severe intrusions due to high roughness, resulting in deep valleys. The inconsistency of these outcomes is clearly due to the different post-processing the parts underwent: machining and refining by grinding in the present work, just sandblasting in literature⁹⁻¹⁰, which resulted in a much higher roughness. Moreover, a small amount of porosities was observed in the previous studies⁹⁻¹⁰, with even no porosity being retrieved in the microscope observation of the fracture surfaces. The research work¹¹ is particularly interesting, as it deals with fatigued Ti-6Al-4V samples, where a remarkable amount of porosities and voids was artificially induced by an improper process parameter setting. The presence of voids and a poor penetration during the stacking process prevented a complete fusion between the overlapped layers. Microscope observation indicate that, unlike the previous case, cracks propagated from subsurface voids, which indicates they indeed acted as stress risers.

Finally, the occurred failure mechanism was compared to that described in the research¹ that deals with the same AISI 18Ni300 Maraging steel. In that case, heat-treated and polished axisymmetric samples underwent low-cycle fatigue tests in strain-controlled conditions by an axial testing machine. The fracture surfaces of the specimens were subsequently examined by scanning electron microscope. The outcomes of this analysis indicate that sub-surface defects, such as voids in the material, due to unmolten powder particles, acted as crack triggers. The presence of unmolten particles is often caused by lack of penetration of the molten pool into the substrate of previously deposited layers. Therefore, for almost all the samples, the fatigue crack initiated from the surface or from defects being located just beneath it and then propagated up to complete part separation. It is interesting to remark that the image in literature¹ of the crack surface in the initiation area indicates a very similar failure mechanism to that observed in the present study. It suggests that lack of penetration is likely to be the primary reason for the porosities that triggered almost the totality of the occurred failures.

The outcomes of the carried out micrographies are shown in the pictures in Fig. 6 with reference to samples of Set #4 that were horizontally stacked with a 3 mm allowance. The deposited layers are visible in Fig. 6 (a): this image was recorded, considering a cut along the sample cross section. The laser scans along the build plane are then visible in Fig. 6 (b): this picture was taken, following a cut along a plane containing the sample longitudinal axis, i.e. along the deposition plane. Circles are used in both the pictures to highlight the defects, mainly consisting in inclusions. These were always located at the interfaces between adjacent layers or laser scans, regardless of the build orientation and of other allowance features. This outcome can also be observed in Figs. 6 (c) and (d), where approximately $5\mu\text{m}$ large inclusion at the interstices between adjacent layers are visible. The microstructure of the studied Maraging steel is generally formed by elongated grains being about $80\mu\text{m}$ long and $20\text{-}30\mu\text{m}$ wide. Moreover, it is also possible to remark the presence of martensitic needles, which are highlighted by arrows in Figs. 6 (c) and (d), considering part cross section along the stacking direction and in Figs. 6 (e) and (f), where the microstructure on the build plane is

depicted. The observed structure is also well consistent with that described in literature¹, where the same material in the not heat treated state was studied.

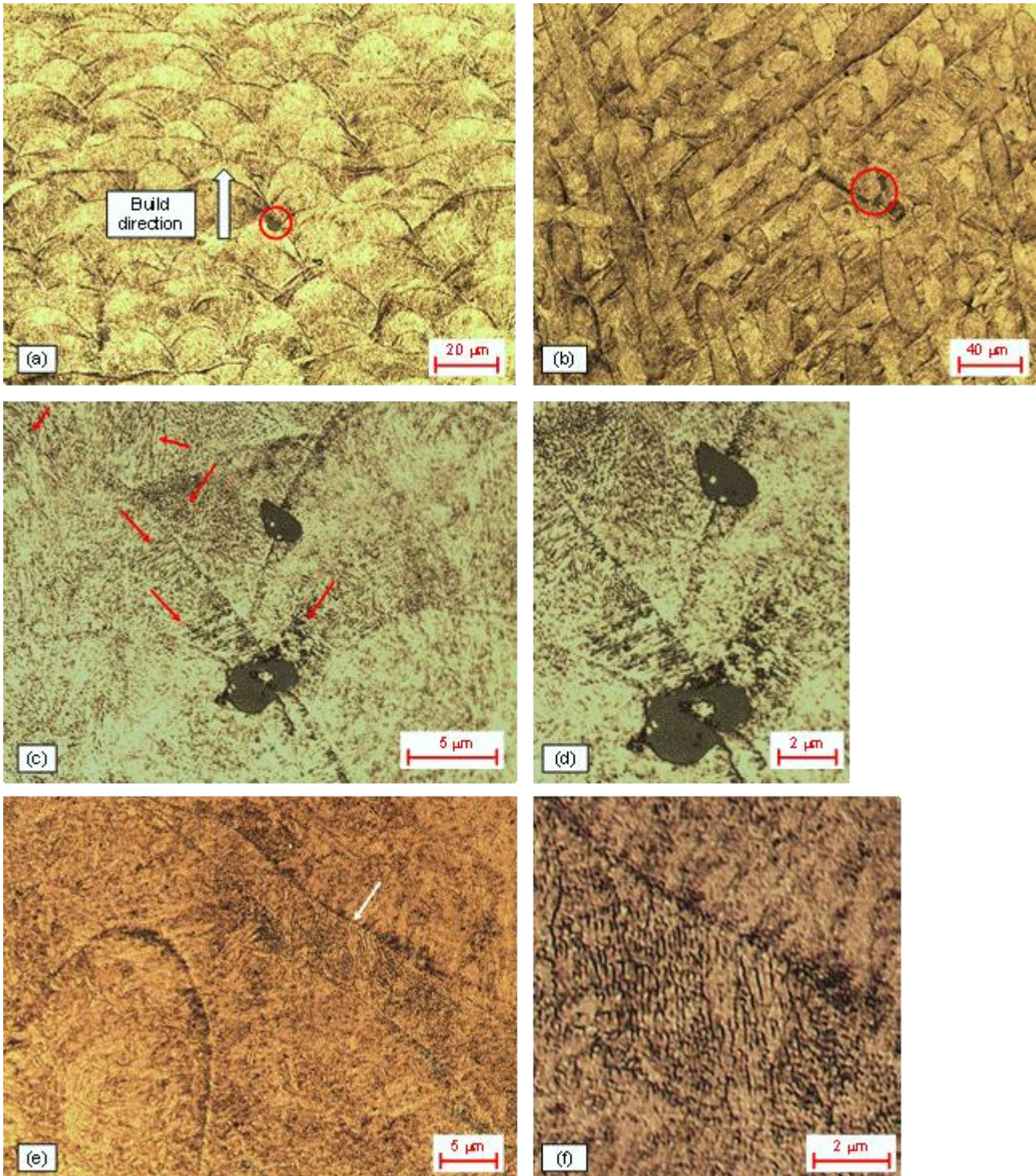


Fig. 6: Micrographies on samples of Set #4 (H,3): (a) stacked layers with highlighted build direction (emphasized inclusions by red circles); (b) laser scans, (emphasized inclusions by red circles); (c) inclusions at the interface between adjacent layers with arrows pointing to martensitic needles; (d) enlarged detail; (e) martensitic needles between laser scans indicated by an arrow; (f) enlarged detail

CONCLUSIONS

This study has been focused on the fatigue response of aged Maraging steel MS1 (also reported as 18% Ni Maraging 300 or AISI 18Ni300). In particular, the possible effect of build orientation and of the allowance for machining have been addressed.

The aforementioned goals have been tackled experimentally and the results, statically processed, have indicated that the two mentioned factors do not have any impact on the fatigue response. In particular, the averaged fatigue limit, including all the performed tests, is 581 MPa, corresponding to 28% of the Ultimate Tensile Strength. This completely isotropic response is due to the beneficial effect of aging and machining, to the higher layer thickness (with respect, for instance to Stainless Steels) and to material properties, especially a not high coefficient of thermal expansion, which lead to a quite small residual stress field arising from the stacking process.

The analysis has been completed by the determination of a global fatigue curve that can be regarded as one of the most general and reliable models for fatigue life prediction of Maraging Steel MS1 in the current literature. This curve, along with its confidence band, has been determined through the interpolation of 56 experimental data. Analytical equations, for 50%, 10% and 90% failure probabilities have been provided as well.

Finally, fractographic analyses have been conducted and have indicated that cracks usually start from sub-surface porosities having dimensions and distance from the edge of respectively 50 μ m and 80 μ m, and presumably due to lack of penetration. Martensitic needles and some inclusions at the interfaces between adjacent layers and laser scans have also been highlighted by micrographies conducted on the build plane and along the perpendicular build direction.

ACKNOWLEDGEMENTS

The research presented in this paper has received funding from the European Union's Horizon 2020 research and innovation programme under the Marie Skłodowska-Curie grant agreement No. 734455.

REFERENCES

1. Branco R, Costa JDM, Berto F, Razavi SMJ, Ferreira JAM, Capela C, et al. Low-Cycle Fatigue Behaviour of AISI 18Ni300 Maraging Steel Produced by Selective Laser Melting. *Metals*. 2018; 8 (32): 1-15.
2. Becker TH, Dimitrov D. The achievable mechanical properties of SLM produced Maraging Steel 300 components. *Rapid Prototyp J*. 2016; 22 (3): 487-494.
3. Croccolo D, De Agostinis M, Fini S, Olmi G, Bogojevic N, Ciric-Kostic S. Effects of build orientation and thickness of allowance on the fatigue behaviour of 15–5 PH stainless steel manufactured by DMLS. *Fatigue Fract Eng Mater Struct*. 2018; 41: 900-916.
4. Herderick E. Additive Manufacturing of Metals: A Review. *In Proc. of Materials Science and Technology (MS&T)*. Columbus, Ohio; 2011: 1413-1425.
5. Lewandowski JJ, Seifi M. Metal Additive Manufacturing: A Review of Mechanical Properties. *Annu Rev Mater Res*. 2016; 46: 151-186.
6. Nicoletto G. Directional and notch effects on the fatigue behavior of as-built DMLS Ti6Al4V. *Int J Fatigue*. 2018; 106: 124-131.

7. Abe F, Osakada K, Shiomi M, Uematsu K, Matsumoto M. The manufacturing of hard tools from metallic powders by selective laser melting. *J Mater Process Technol.* 2001; 111 (1-3): 210-213.
8. Santos EC, Shiomi M, Osakada K, Laoui T. Rapid manufacturing of metal components by laser forming, *Int J Mach Tool Manu.* 2006; 46 (12-13): 1459-1468.
9. Razavi SMJ, Ferro P, Berto F, Torgersen J. Fatigue strength of blunt V-notched specimens produced by selective laser melting of Ti-6Al-4V. *Theor Appl Fract Mec.* (In Press); DOI: 10.1016/j.tafmec.2017.06.021.
10. Razavi SMJ, Ferro P, Berto F (2017). Fatigue Assessment of Ti-6Al-4V Circular Notched Specimens Produced by Selective Laser Melting. *Metals.* 2017; 7 (291): 1-10.
11. Razavi SMJ, Bordonaro GG, Ferro P, Torgersen J, Berto F. Fatigue Behavior of Porous Ti-6Al-4V Made by Laser-Engineered Net Shaping. *Materials.* 2018; 11 (284): 1-8.
12. Niemann G, Winter H, Hohn BR. *Maschinenelemente.* Berlin, Germany: Springer-Verlag; 2005..
13. Casati R, Lemke J, Vedani M. Microstructural and Mechanical Properties of As Built, Solution Treated and Aged 18 Ni (300 grade) Maraging Steel Produced by Selective Laser Melting. *Metall Ital.* 2017; 1: 11-20.
14. https://cdn0.scrvt.com/eos/c88047245bff2c4b/2f494ef432d0/MS-MS1-M280_M290_400W_Material_data_sheet_05-14_en.pdf
15. Croccolo D, De Agostinis M, Fini S, Olmi G, Vranic A, Ciric-Kostic S. Influence of the build orientation on the fatigue strength of EOS maraging steel produced by additive metal machine. *Fatigue Fract Eng Mater Struct.* 2016; 39: 637-647.
16. Karlinski W, Tacikowski J, Wojtyra K. Fatigue strength of nitrided 18Ni250 and 18Ni300 grade maraging steels. *Surf Eng.* 1999; 15: 483-489.
17. Nagano T, Kawagoishi N, Moriyama M, Chen Q, Nagashima E. Influence of shot peening on fatigue strength of maraging steels with different hardness. *J Soc Mater Sci.* 2007; 56: 1126-1132.
18. Wang W, Yan W, Duan Q, Shan Y, Zhang Z, Yang K. Study on fatigue property of a new 2.8 GPa grade maraging steel. *Mater Sci Eng B.* 2010; 527: 3057-3063.
19. Chen, Q, Nagano T, Nakamura Y, Maeda Y, Kawagoishi N. Initiation and propagation behavior of a fatigue crack of maraging steel in high humidity. *In: Proceedings of 13th International Conference on Fracture, International Congress on Fracture (ICF).* Beijing, China; 2013: 16-21.
20. Schuller R, Fitzka M, Irrasch D, Tran D, Pennings B, Mayer H. VHCF properties of nitrided 18Ni maraging steel thin sheets with different Co and Ti content. *Fatigue Fract Eng Mater Struct.* 2015; 38: 518-527.
21. Santos LMS, Ferreira JAM, Jesus JS, Costa JM, Capela C. Fatigue behaviour of selective laser melting steel components. *Theor Appl Fract Mec.* 2016; 85: 9-15.
22. Mutua J, Nakata S, Onda T, Chen Z-C. Optimization of selective laser melting parameters and influence of post heat treatment on microstructure and mechanical properties of maraging steel. *Mater Design.* 2018; 139: 486-497.
23. Zhang X, Martina F, Ding J, Wang X, Williams S. Fracture toughness and fatigue crack growth rate properties in wire + arc additive manufactured Ti-6Al-4V. *Fatigue Fract Eng Mater Struct.* 2017; 40 (5): 790-803.

24. Zhang J, Wang X, Paddea S, Zhang X. Fatigue crack propagation behaviour in wire+arc additive manufactured Ti-6Al-4V: effects of microstructure and residual stress. *Mater Design*. 2016; 90: 551-561.
25. Van Hooreweder B, Moens D, Boonen R, Kruth J-P, Sas P. Analysis of fracture toughness and crack propagation of Ti-6Al-4V produced by selective laser melting. *Adv Eng Mater*. 2012; 14: 92-97.
26. Wycisk E, Siddique S, Herzog D, Walther F, Emmelmann C. Fatigue performance of laser additive manufactured Ti-6Al-4V in very high cycle fatigue regime up to 10^9 cycles. *Front Mater*. 2015; 2: 1-8.
27. Tan C, Zhou K, Ma W, Zhang P, Liu M, Kuang T. Microstructural evolution, nanoprecipitation behavior and mechanical properties of selective laser melted high-performance grade 300 maraging steel. *Mater Design*. 2017; 134: 23-34.
28. Dixon WJ, Massey F Jr. *Introduction to Statistical Analysis*. New York, United States: McGraw-Hill; 1983.
29. Olmi G, Comandini M, Freddi A. Fatigue on shot-peened gears: experimentation, simulation and sensitivity analyses. *Strain*. 2010; 46 (4): 382-395.
30. Olmi G, Freddi A. A new method for modelling the support effect under rotating bending fatigue: application to Ti-6Al-4V alloy, with and without shot peening. *Fatigue Fract Eng Mater Struct*. 2013; 36 (10): 981-993.
31. Van Hooreweder B, Moens D, Boonen R, Sas P. The critical distance theory for fatigue analysis of notched aluminium specimens subjected to repeated bending. *Fatigue Fract Eng Mater Struct*. 2012; 35: 878-884.
32. International Organization for Standardization ISO 12107:2012. *Metallic Materials – Fatigue Testing – Statistical Planning and Analysis of Data*. Geneva, Switzerland: International Organization for Standardization (ISO) ; 2012.
33. Olmi G. Low Cycle Fatigue Experiments on Turbogenerator Steels and a New Method for Defining Confidence Bands. *J Test Eval*. 2012; 40 (4): Paper ID JTE104548.
34. Fergani O, Berto F, Welo T, Liang SY. Analytical modelling of residual stress in additive manufacturing. *Fatigue Fract Eng Mater Struct*. 2017; 40: 971-978.